Journal of Sound and Vibration (1998) **213**(5), 813–827

WAVELET BASED CUTTING STATE IDENTIFICATION

B. S. Berger, I. Minis, J. Harley, M. Rokni and M. Papadopoulos

Department of Mechanical Engineering, University of Maryland, College Park, MD 20742-3035, *U.S.A.*

(*Received* 18 *July* 1997, *and in final form* 30 *December* 1997)

Chatter and non-chatter cutting states, associated with the orthogonal cutting of stiff metal cylinders, are identified through an analysis of the ratios of the mean absolute deviations of details of the biorthogonal 6,8 wavelet decomposition of cutting force measurements. Sequences of cutting experiments were performed in which either depth of cut or turning frequency was varied. For light and medium cutting the mean absolute deviations of the ratios of details d_3 and d_4 is less than 7 while for chatter it is greater than 15. The kurtosis of detail d_3 is shown to identify transitions to chatter.

1. INTRODUCTION

The construction of models of orthogonal cutting from first principles presents problems which have not, as yet, been entirely resolved. A review of cutting vibration research to 1979 is given in reference [1]. Examples of more recent modelling are provided in references [2, 3].

Contemporary efforts to control cutting dynamics have emphasized signal processing methodologies in an attempt to avoid the difficulties inherent in the construction of physical models. Back propagation neural networks were used to detect the onset of chatter in reference [4]. Cutting state characterization by other means was required before numerically generated functions could be constructed to train the neural networks.

Gaussian wavelet transforms were employed in reference [5] to study the dynamical characteristics of non-regenerative thread and slot cutting processes. Tool acceleration and cutting forces were measured for feeds parallel and perpendicular to the rotational axis of a turning specimen. The effects of spindle speed, feed rates and width of cut were studied. Differentiation between various cutting states was made on the basis of qualitative features of power spectra and wavelet based time frequency plots. Real time or simulated control of the cutting process was not reported. In reference [6] algorithms based on higher order spectral analysis were applied to state identification in orthogonal cutting.

In the following the identification of chatter and pre-chatter states associated with the orthogonal cutting of stiff cylinders is realized through an analysis of the ratio of the mean absolute deviations of details d_3 and d_4 of a biorthogonal 6,8, bi 6,8, wavelet decomposition of cutting force measurements. An examination of the bi 6,8 decomposition of cutting force measurements revealed systematic changes in the amplitudes of details d_3, d_4. Since algorithms for on-line real time control are sought, computationally simple and efficient measures of amplitude were considered. The standard deviation, mean absolute deviation and median absolute deviation were studied. Amongst these the ratio of the mean absolute deviation of details d_3 and d_4, m.a.(3,4), was found to provide a consistent identification

0022–460X/98/250813 + 15 $25.00/0/sv971495

of pre-chatter and chatter states. Because of the relatively high noise levels associated with tool acceleration data, the m.a.(3,4) ratio was found to be a less effective indicator of cutting states when based on tool acceleration data rather than on cutting force data. The kurtosis of d_3 was computed and identified as useful in characterizing transitions to chatter.

Sequences of cutting experiments were performed in which either depth of cut or turning frequency was varied with all other cutting parameters held constant. Each variable cutting depth sequence ended in chatter while each variable turning frequency sequence contained at least one chatter state. Three sequences of experiments with variable depth of cut and two with variable turning frequency, a total of 24 cutting experiments, were studied. Results typical of the entire set are presented for two sequences of variable cutting depth and a single sequence of variable turning frequency. For light and medium cutting m.a.(3,4) < 7. For chatter m.a.(3,4) > 15. In a 5-s transition to chatter for constant depth of cut and turning frequency, m.a.(3,4) monotonically increased from 8·0 to a maximum of 18·0 at chatter.

Wavelets possess excellent resolution capabilities in the time domain which is advantageous in the analysis of non-stationary time series arising in metal cutting. The ratio m.a.(3,4) was computed over 1-s intervals of the time series. However, similar results were found for intervals of 0·5 s.

A description of the experimental apparatus is followed by definitions and results from the theory of biorthogonal wavelets. Measures of the amplitudes of details, d_i, of wavelet decompositions are presented and applied to the analysis of the cutting data. A study of sequences of cutting experiments shows that the ratio m.a.(3,4) differentiates between chatter, pre-chatter and other cutting states.

2. EXPERIMENTAL APPARATUS

A schematic diagram of the experimental apparatus employed is shown in Figure 1 and consists of a Hardinge CNC lathe, a special force dynamometer (utilizing three Kistler

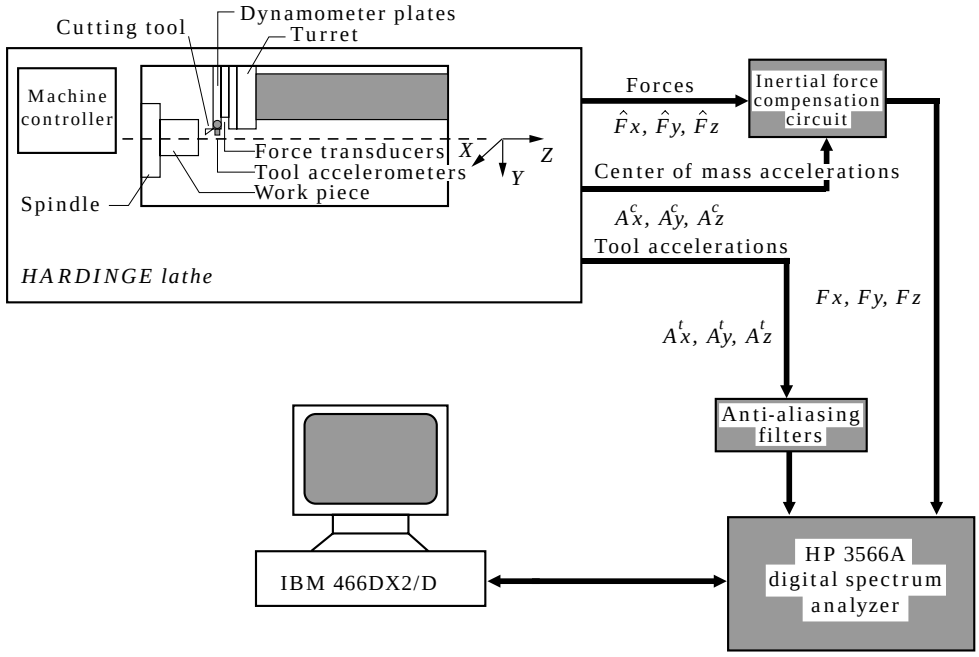

Figure 1. The experimental system.

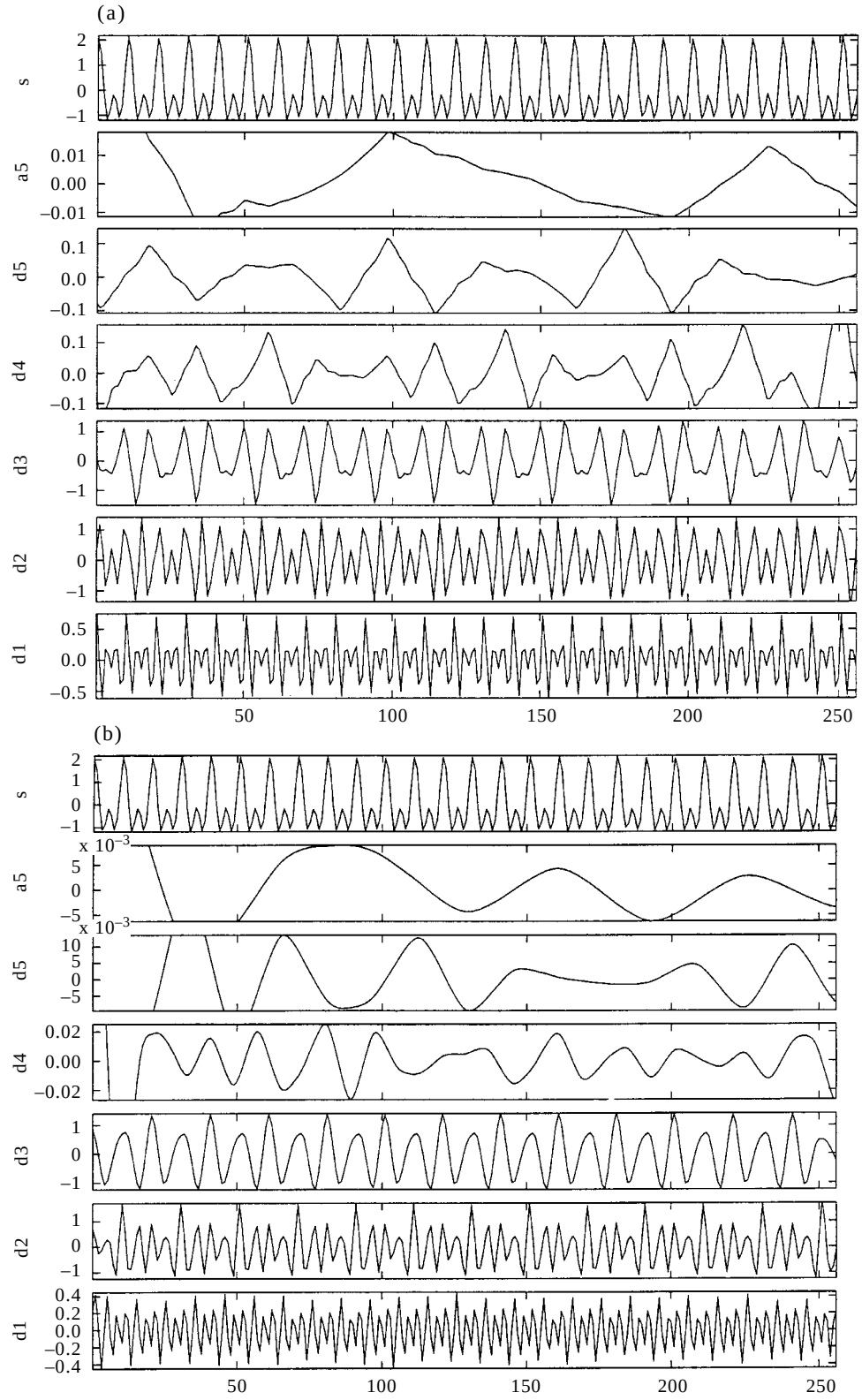

Figure 2. Test function $f_1(x)$: (a) level 5 db3 decomposition of f_1; (b) level 5 bi 6,8 decomposition of f_1; amplitude versus data point number.

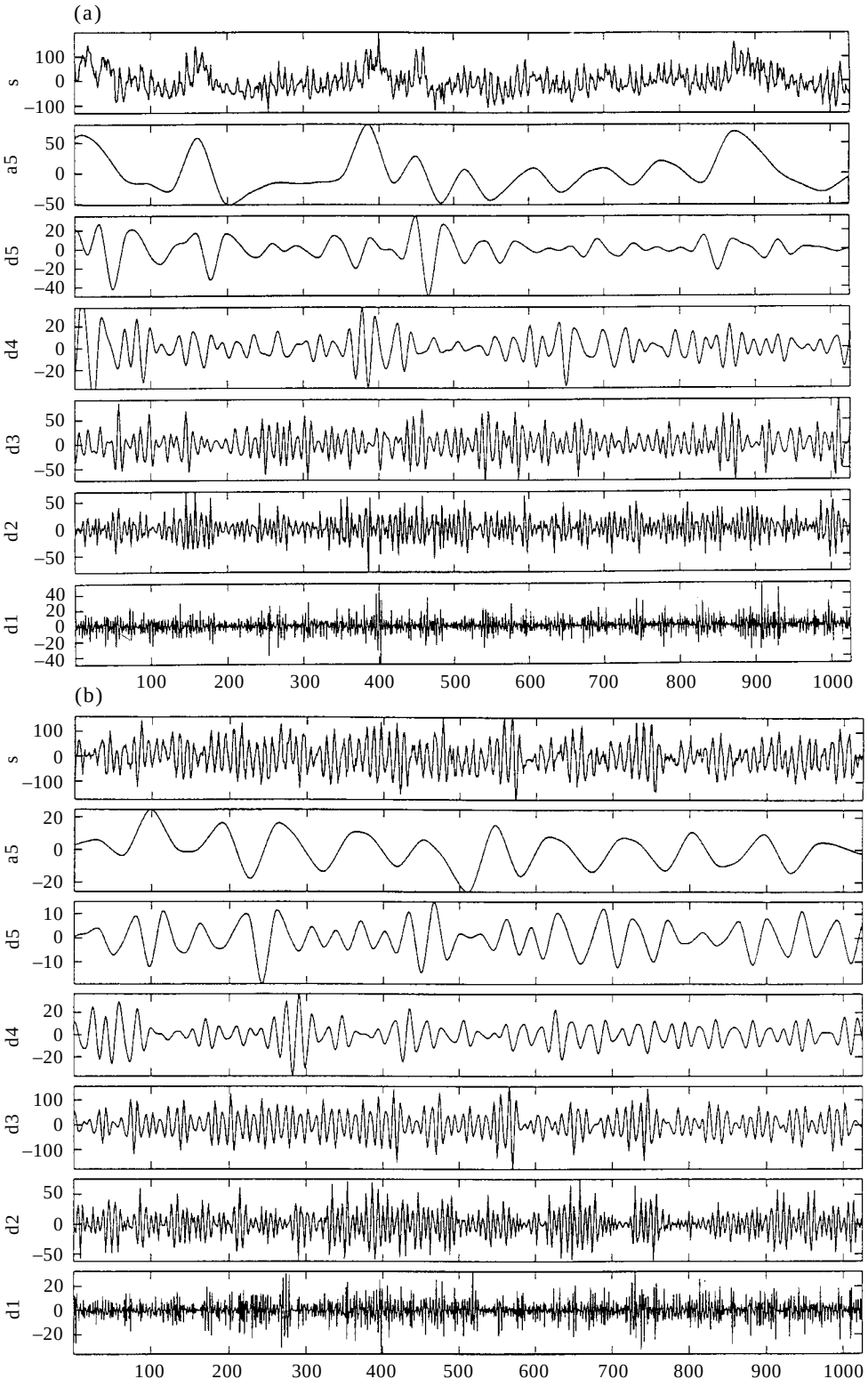

Figs 3(a) and (b)—*Caption opposite*.

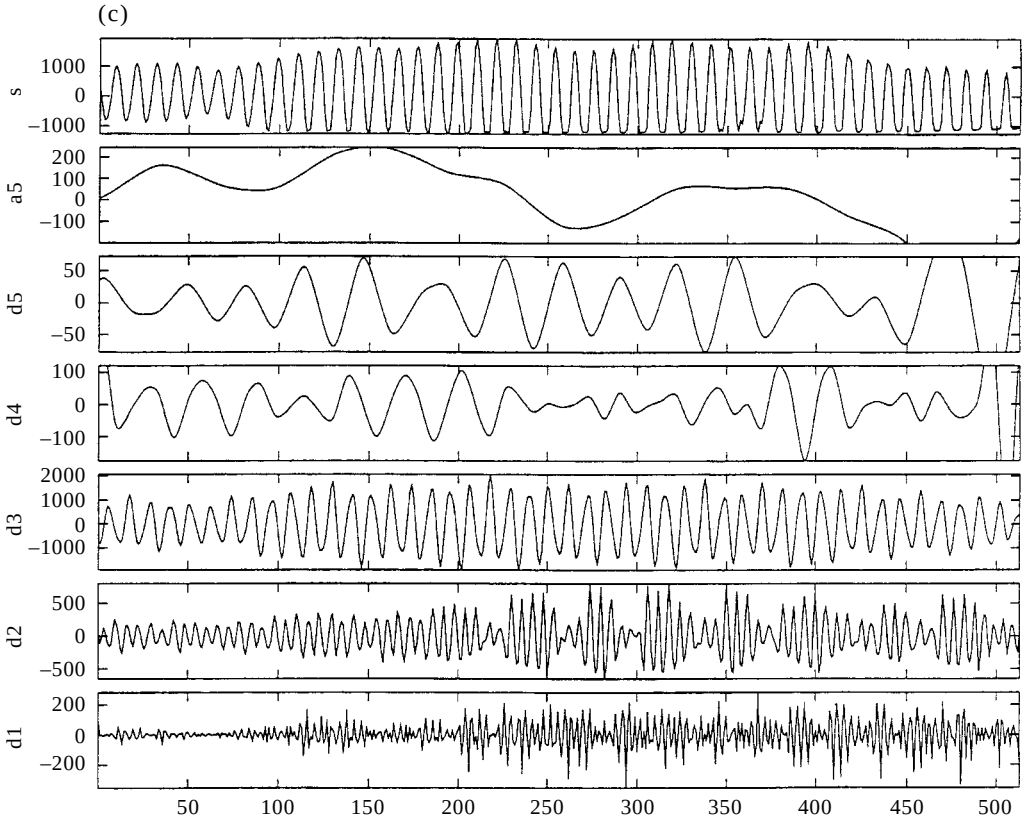

Fig. 3(c).

Figure 3. Bi 6,8 decomposition at level 5 of s-1; (a) 2·3 mm; (b) 2·6 mm; (c) 2·8 mm; amplitude versus data point number.

9068 force transducers) and its associated electronics, and a digital spectrum analyzer (Hewlett Packard 3566A) for data acquisition and real-time analysis.

All experiments involve only right-handed orthogonal cutting. Positive rake tool inserts were employed (Kennametal TPMR322) and were supported by Kennametal KT-GPR123B tool holders. The tool holder–insert combination resulted in a rake angle of 5° and a clearance angle of 4°. Cylindrical work pieces of 1020 steel were machined under a wide range of cutting conditions.

Tool flank wear was held to less than 0·1 mm. The feed rate was constant with a value of 0·007 ipr. (0·1778 mm/rev) and identical for every experiment. A constant cutting speed of 90 m/min was realized for experiments with various turning frequencies by utilizing workpieces of suitably chosen diameters.

The force dynamometer is rigidly mounted on the lathe's turret and is specifically designed for compatibility with its geometry. It comprises three Kistler 9068 tri-axial force transducers sandwiched between heavy steel plates under high pre-load. The cover plate is an exact copy of the turret's channel design capable of carrying ordinary left and right handed tools. The lowest natural frequency of the assembly is approximately 6000 Hz and the maximum allowable amplitude for each component of the applied cutting force is 13 kN (2923 lbf). Compensation of the force measurements of the inertia of the top plate of the dynamometer assembly is carried out by an analogue circuit utilizing the measured accelerations of the centre of mass of the plate.

Since all work pieces were stubby, work piece modal characteristics did not affect the turning dynamics. The sampling rate was 4096 Hz and the cut off frequency was 1100 Hz. Record lengths ranged from 20–60 s except for chatter records which had a duration of 2–10 s.

3. BIORTHOGONAL WAVELETS

The dual biorthogonal wavelet bases $\Psi_{jk}^{(\alpha)}$, $\alpha = 1,2$, are each given by the dilates and translates of dual wavelet functions $\Psi^{(\alpha)}$, respectively, with $\Psi^{(\alpha)} \in L^2(R)$ and

$$\Psi_{jk}^{(\alpha)}(x) = 2^{-j/2}\Psi^{(\alpha)}(2^{-j}x - k). \tag{1}$$

The Fourier transforms of the dual scaling functions are

$$\hat{\phi}^{(\alpha)}(\xi) = (2\pi)^{-1/2}\prod_{j=1}^{\infty} m_0^{(\alpha)}(2^{-j}\xi), \tag{2}$$

where

$$m_0^{(\alpha)}(\xi) = 2^{-1/2}\sum_n h_n^{(\alpha)} \exp(-i \quad n \quad \xi), \qquad \sum_n h_n^{(1)} h_n^{(2)} + 2k = \delta_{ko} \tag{3, 4}$$

and

$$\hat{\phi}(\xi) = (2\pi)^{-1/2}\int \exp(-i \quad \xi \quad x)\phi(x)\,\mathrm{d}x. \tag{5}$$

The dual wavelet and scaling functions are related by

$$\psi^{(\alpha)}(x) = \sqrt{2}\sum_n (-1)^n h_{1-n}^{(\alpha)}\phi^{(\alpha)}(2x + n). \tag{6}$$

It is then shown in references [7, 8] that for any $f \in L^2(R)$,

$$f(x) = \sum_{j,k} < f, \psi_{jk}^{(\alpha)} > \psi_{jk}^{(\beta)}(x), \tag{7}$$

with $\alpha, \beta = 1, 2$ and $\alpha \neq \beta$ provided there exists C and ε so that $|\hat{\phi}^{(\alpha)}(\xi)| \leqslant C(1 + |\xi|)^{-1/2-\varepsilon}$ and $\int \phi^{(\alpha)}(x)\phi^{(\beta)}(x - k)\,\mathrm{d}x = \delta_{ko}$, where $\langle fg \rangle = \Sigma f(n)g(n)$.

In the biorthogonal case it is possible to choose $m_0^{(1)}$ so that the associated scaling function is symmetric, $\phi^{(1)}(x) = \phi^{(1)}(-x)$. The filter associated with $m_0^{(1)}$ is then a linear phase filter [7, 8] for which

$$m_0^{(1)}(\xi) = \exp(i \quad \lambda \quad \xi)|m_0^{(1)}| \tag{8}$$

for some real λ. Wavelets associated with symmetric scaling functions or linear phase are found to be smooth [7].

The result (7) was essentially derived in reference [9] through the theory of filter banks. Conditions for perfect reconstruction of the given time series, $f(n)$, are also proven.

The cutting data wavelet analysis was carried out utilizing biorthogonal wavelets associated with the 6,8 spline scaling functions. For this case $\phi^{(1)}$ and $\phi^{(2)}$ are sixth and eighth order B-spline functions, respectively. The family of biorthogonal wavelets based on the B-spline functions was developed in references [7, 9] and implemented in reference [10].

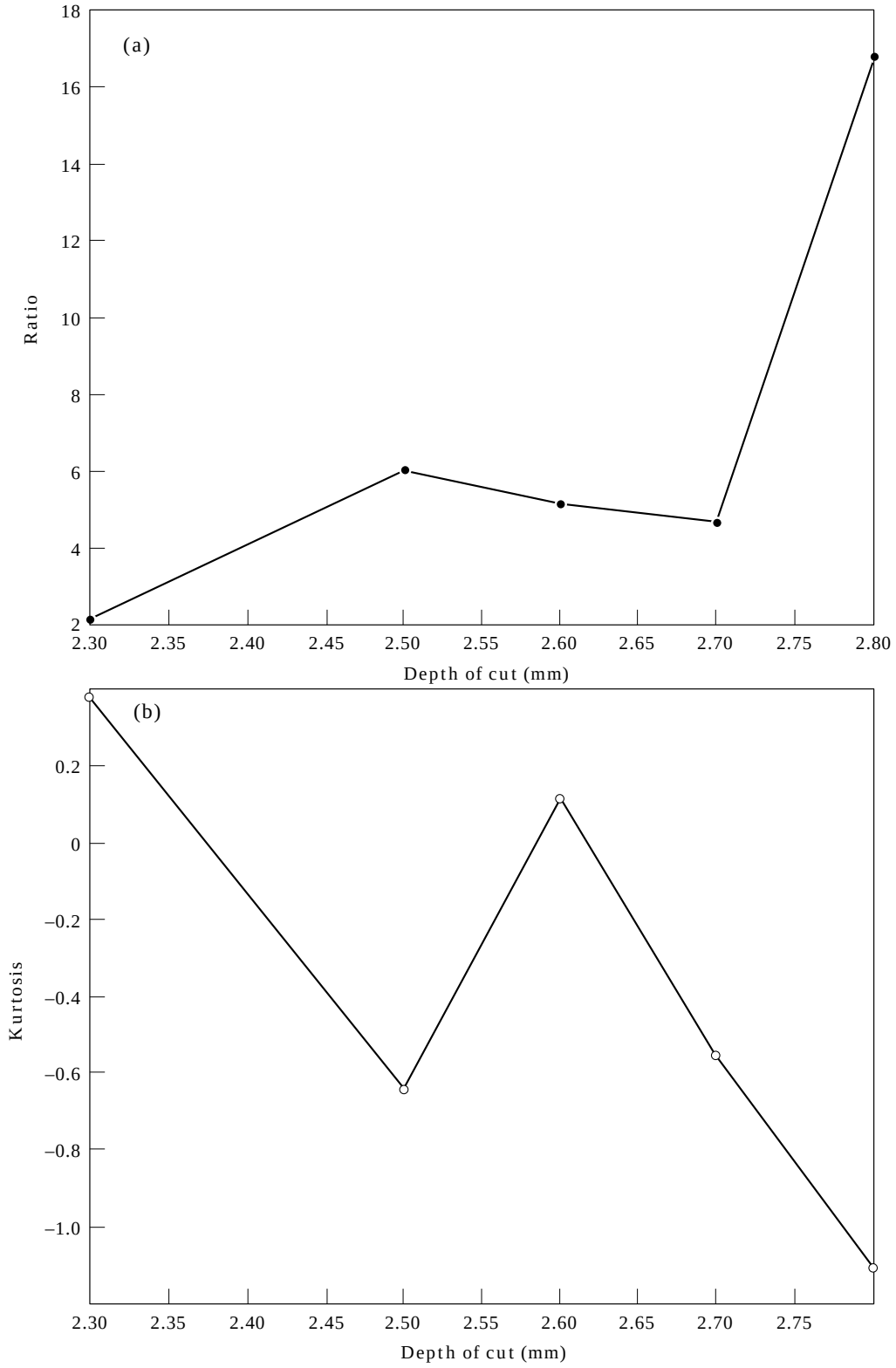

Figure 4. (a) m.a.(3,4) versus depth of cut for s-1; (b) kurtosis versus depth of cut for s-1.

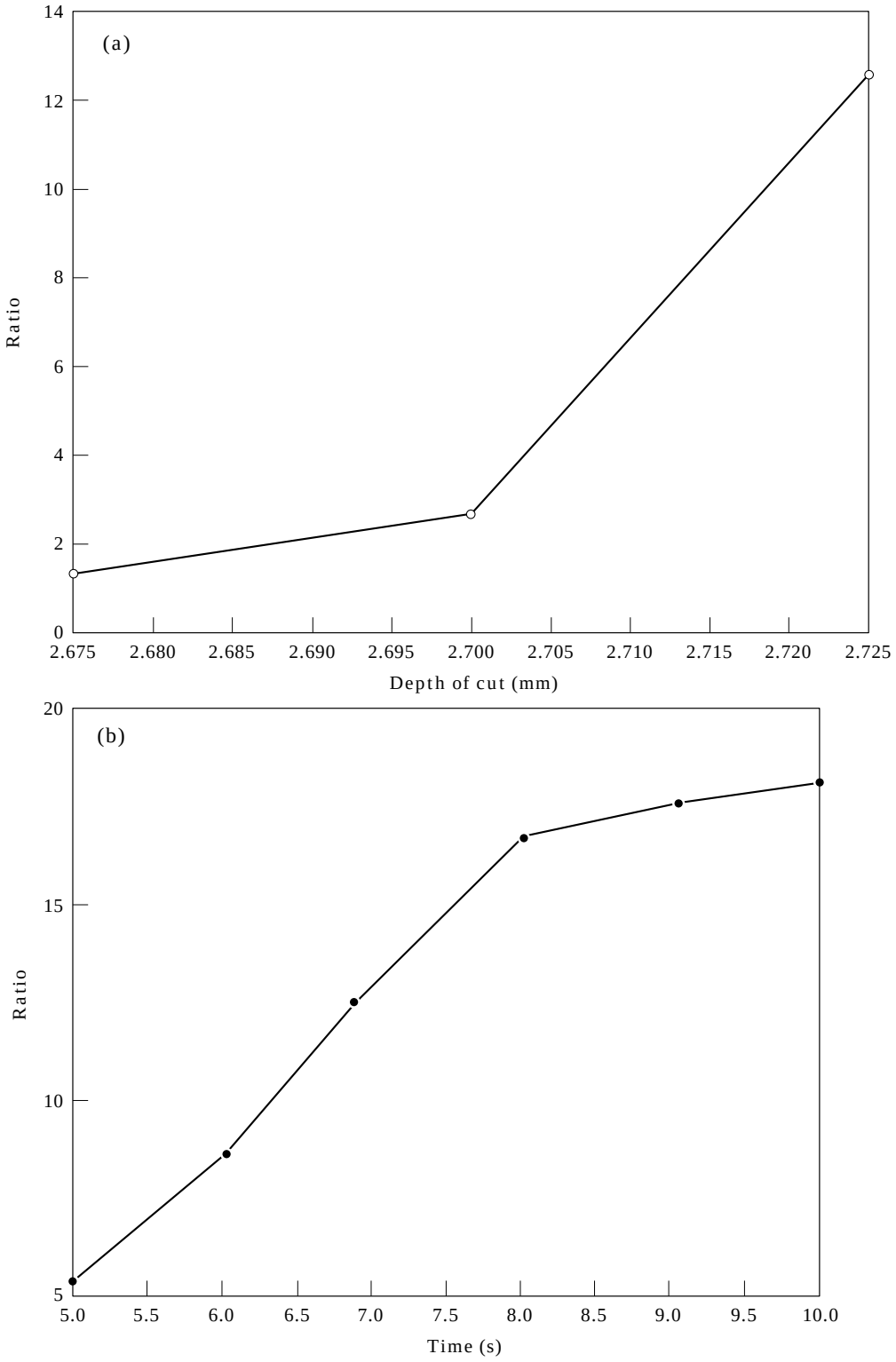

Figs 5(a) and (b)—*Caption on opposite page*.

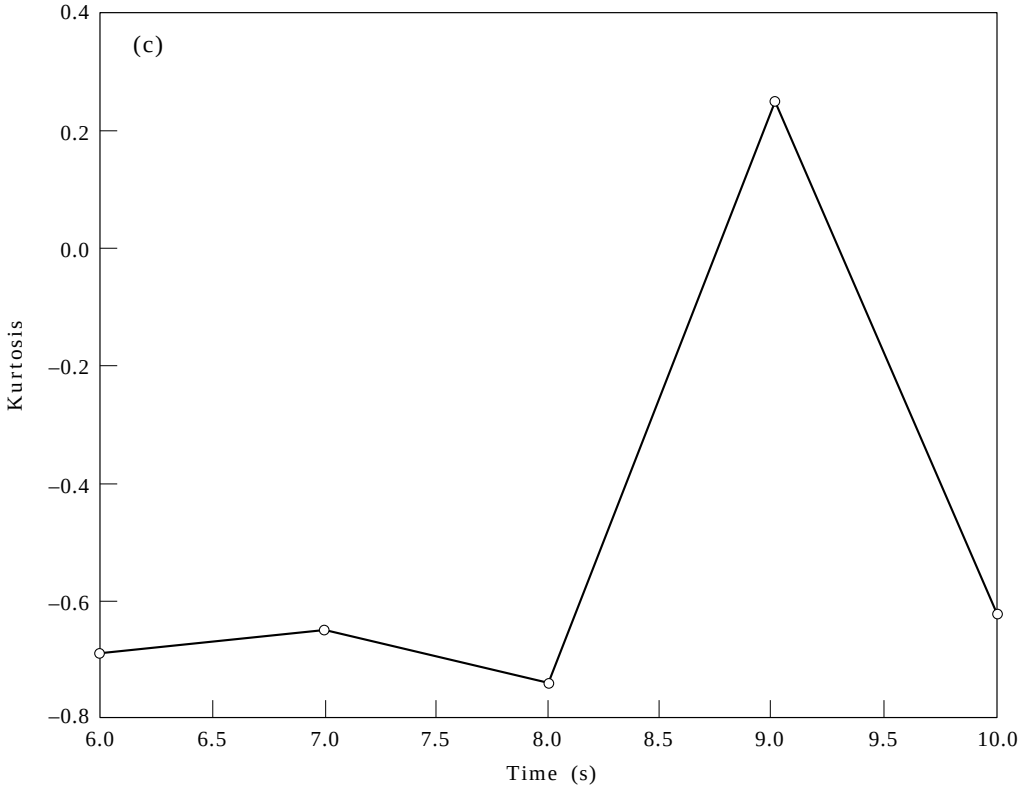

Figure 5. (a) m.a. (3,4) versus depth of cut for s-2; (b) m.a. (3,4) versus depth of cut for the s-2 transition to chatter; (c) kurtosis versus depth of cut for the s-2 transition to chatter.

The choice of the 6,8 biorthogonal wavelet for subsequent time series analysis was the result of a numerical study of analytic test cases and cutting force time series with the Daubechies and spline based biorthogonal wavelet families. It is shown in reference [8] that the biorthogonal wavelet 6,8 has bounded support, perfect reconstruction and linear phase.

A detail, $d_j(x)$, of a function $f(x)$, is defined as

$$d_j(x) = \sum_k < f, \psi_{jk}^{(\alpha)} > \psi_{jk}^{(\beta)}(x) \tag{9}$$

and an approximation A_N at the Nth level [10], by

$$A_N = \sum_{j>N} d_j. \tag{10}$$

Then for a perfect reconstruction at the Nth level of the discreet function $f(n)$ [8, 11],

$$f(n) = A_N + \sum_{j \leqslant N} d_j. \tag{11}$$

The Daubechies 3, db3, and 6,8 biorthogonal, bi 6,8, decompositions of the phase coupled function

$$f_1(x) = \cos(0{\cdot}2\pi t + \phi_1) + \cos(0{\cdot}2\pi t + \phi_2) + \cos(0{\cdot}4\pi t + \phi_1 + \phi_2) \tag{12}$$

are shown in Figures 2(a) and (b), respectively. $\phi_1(t)$ and $\phi_2(t)$ are independent, uniformly distributed random variables. The smoothing and resolution capabilities of bi 6,8 for equation (12) are evident from a comparison of Figures 2(a) and (b). An examination of the amplitudes indicates superior resolution and smoothing of d_i in the case of bi 6,8. Bi 6,8 is subsequently used for the decomposition of time series derived from the single point cutting of steel cylinders.

4. AMPLITUDE ESTIMATION

An examination of the decomposition of data set s-1, Figures 3(a)–(c) reveals systematic changes in the amplitudes of the details, d_i, equation (9). For example, the amplitude of d_3 increases as a function of the depth of cut. The standard, mean absolute and median absolute deviations were chosen as readily computed measures of amplitude. Given a data set x_i, $i = 1, n$ with mean $\mu = (\Sigma x_i)/n$, median $\equiv \delta$, standard deviation $\equiv \sigma$, mean absolute deviation $\equiv$ m.a. where

$$\text{m.a.} = \frac{1}{n}\sum_i |x_i - \mu|, \tag{13}$$

Measure of the departure of the distribution of set x_i from a normal distribution around the mean is provided by the kurtosis $\equiv \gamma_2$, where

$$\gamma_2 = (\mu_4/\sigma^4) - 3, \tag{14}$$

with $\mu_4 = (1/n)\Sigma(x_i - \mu)^4$. $\gamma_2 = 0$ for a normal distribution. The kurtosis has been found to be useful in characterizing transitions into chatter. If $x = \sin t$ for $0 \leqslant t \leqslant 2m\pi$, where m is an integer, then $\gamma_2 = -1{\cdot}5$. For the function $x = 1$, $0 \leqslant t \leqslant 1$, $x = -1$, $-1 < t \leqslant 0$ and $x = 0$ otherwise, $\gamma_2 = -2{\cdot}0$. The histograms for d_3 for chatter and near chatter cutting states resemble those of these two test functions and are similarly associated with negative values of kurtosis, $\gamma_2 < 0$, see equation (14).

5. WAVELET ANALYSIS OF CUTTING DATA

Sequences of cutting experiments were performed in which either depth of cut or turning frequency was varied with all other cutting parameters held constant. Fifth level, $N = 5$, bi 6,8 wavelet decomposition of cutting force measurements are given, over a time interval of 1 s, for two sequences with variable depth of cut and two sequences with variable turning frequency for a turning frequency range of 290–852 r.p.m. Each variable cutting depth sequence ended in chatter while each variable turning frequency sequence contained at least one chatter state. A total of 24 cutting experiments were performed for which cutting forces were measured.

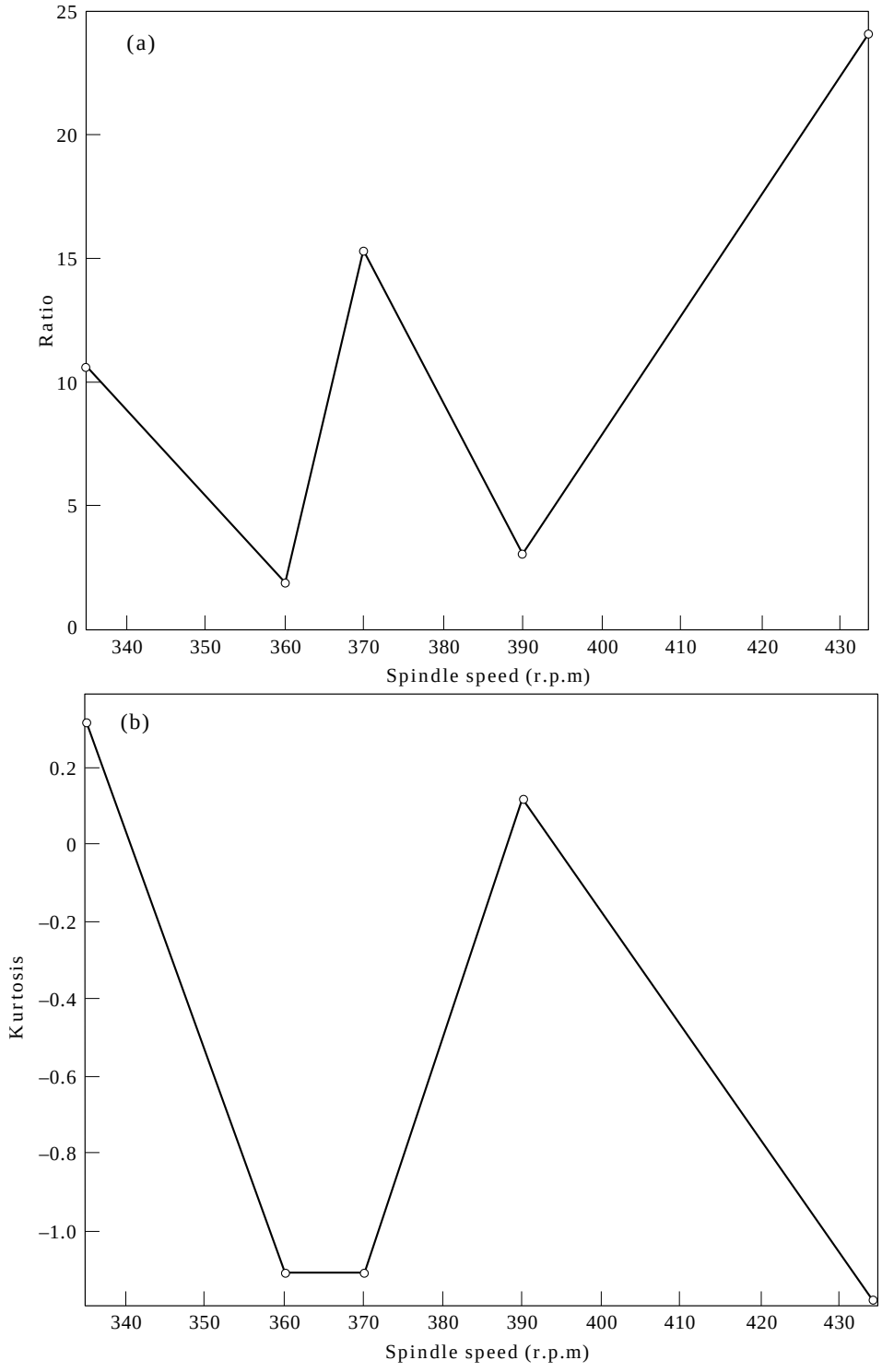

Figure 6. (a) m.a.(3,4) versus turning frequency for s-3; (b) kurtosis versus turning frequency for s-3.

For sequence 1, s-1, the turning frequency = 708 r.p.m., rake angle = 5°, surface speed = 90 m/min, feed rate = 0·007 in./rev/. resampling rate = 1024 Hz, frequency cut-off = 1100 Hz and the depth of cut = 2·3, 2·5, 2·6, 2·7 and 2·8 mm. At a depth of 2·8 mm chatter was observed.

Level 5, bi 6,8 decompositions of the cutting force are shown in Figures 3(a)–(c) for cutting sequence s-1 with depths of cut of 2·3, 2·6 and 2·8 mm, respectively. The σ, m.a. and md.a, (13, 14, 15), of d_3 and d_4, $\sigma(3)$, $\sigma(4)$, m.a.(3), m.a.(4), etc., form the non-dimensional ratios $\sigma(3, 4) = \sigma(3)/\sigma(4)$, m.a.(3, 4) = m.a.(3)/m.a.(4), etc. m.a.(3, 4) is displayed for sequence s-1 in Figure 4(a).

For non-chatter states m.a.(3, 4) is 2·2 for 2·3 mm, rising to approximately 5·0 for 2·5, 2·6, 2·7 mm and increasing to 16·9 for 2·8 mm, the chatter state. Although all the ratios behave in a qualitatively similar manner m.a.(3, 4) was found to be the most reliable indicator of chatter and pre-chatter states. Consequently only m.a.(3, 4) will be utilized subsequently.

Kurtosis, γ_2, equation (14), provides a measure of the departure from a normal distribution. Kurtosis versus depth of cut for data set s-1 is displayed in Figure 4(b). Kurtosis reaches a value of $-1{\cdot}106$ for the chatter state, depth of cut of 2·8 mm and is negative for 2·7 mm. A negative value of kurtosis is seen to occur for a depth of cut of 2·5 mm, well away from the chatter state.

For sequence 2, s-2, the turning frequency = 297 r.p.m., rake angle = 5°, surface speed = 90 m/min, feed rate = 0·007 in./rev., resampling rate = 1024 Hz, frequency cut-off = 1100 Hz and depth of cut = 2·675, 2·70 and 2·725 mm. At a depth of 2·725 mm, chatter was observed after a 10-s transition. m.a.(3,4) versus depth of cut for s-2 is shown in Figure 5(a). For non-chatter states m.a.(3,4) is 1·3 and 2·7 for depth of cut of 2·675 and 2·7 mm, respectively, increasing to 12·6 for a pre-chatter state at 2·725 mm. The transition to chatter occurring at a depth of cut = 2·725 mm is shown in Figure 5(b). For time $\geqslant$5 s, m.a.(3,4) is an increasing function reaching a value of 18·3 in the final chatter state.

For data set s-2 positive values of kurtosis occur for the non-chatter states corresponding to depths of cut of 2·675 and 2·70 mm. At a depth of 2·725 mm, a 10-s transition to chatter occurs. A large positive value of kurtosis occurs for the first second of the transition. The kurtosis is negative for the next 9 s of the transition except for a small positive value for second nine, just prior to the appearance of chatter.

For sequence 3, s-3, the depth of cut = 2·8 mm, rake angle = 5°, surface speed = 90 m/min, feed rate = 0·007 in./rev., resampling rate = 1024 Hz and turning frequency = 335, 360, 371, 390 and 434 r.p.m. Chatter was observed for turning frequencies of 371 and 434 r.p.m. for which m.a.(3,4) equals 15·3 and 24·22, respectively, Figure 6(a). Values of m.a.(3,4) for the non-chatter states corresponding to 335, 360 and 390 r.p.m. are 10·7, 1·9 and 3·06, respectively.

Kurtosis versus depth of cut for data set s-3 is displayed in Figure 6(b). The kurtosis is negative for the chatter states at 371 r.p.m. and at second two of 434 r.p.m. The first second of 434 r.p.m. is a pre-chatter state with a positive kurtosis. A negative value of kurtosis occurs at 360 r.p.m. which is not a chatter state. The kurtosis is positive for the two remaining non-chatter states corresponding to 335 and 390 r.p.m., respectively.

In the instances discussed above, m.a.(3,4), based on cutting force measurements, discriminated between chatter and all other cutting states. For light to medium cutting m.a.(3,4) < 7. The high resolution of bi 6,8, in time and scale, makes possible the detection, as a function of time, of the transition from a non-chatter to the chatter state. Kurtosis is negative for the chatter state. The values of kurtosis associated with the transition from pre-chatter to chatter are generally negative.

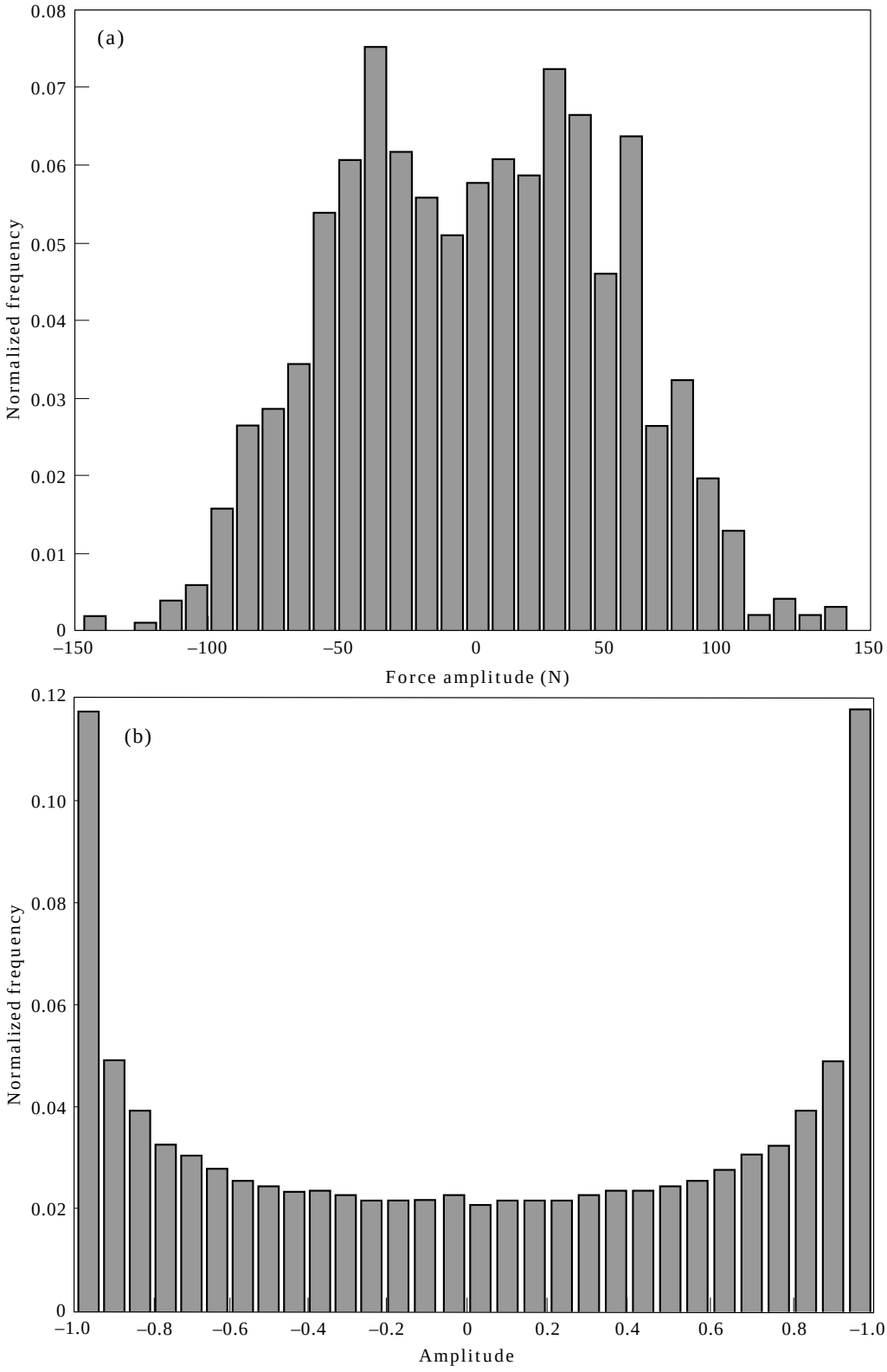

Figure 7. (a) Normalized frequency versus force amplitude for s-1, detail d_3; (b) normalized frequency versus amplitude for $\sin t$.

6. CONCLUSIONS

A wavelet decomposition of cutting force time series is shown to provide a means for the characterization of cutting states. The non-dimensional ratio of the mean absolute deviation of details d_3 and d_4, computed over 1-s intervals of the time series, discriminates between chatter and non-chatter states. In this context the resolving capacity of biorthogonal 6,8 wavelet makes possible the characterization, as a function of time, of the transition from a pre-chatter to the chatter state. Numerical studies indicate that cutting state characterizations over $\frac{1}{2}$ s intervals closely approximate those computed over 1-s intervals. Histograms of d_3 are nearly all bi-modal in the neighborhood of chatter, Figure 7(a). Therefore, the kurtosis of d_3 is almost always negative in such neighborhoods. For the histogram shown in Figure 7(a), data set s-1, depth of cut = 2·8 mm, detail d_3, the kurtosis = $-0{\cdot}88$. Consider the functions $\sin t$, $0 \leqslant t \leqslant 2\pi$ and $f(t) = -1$, $0 \leqslant t < 1$, $+1$, $1 \leqslant t \leqslant 2$ for which the kurtosis equals $-1{\cdot}5$ and $-2{\cdot}0$, respectively. The corresponding histograms are strongly bi-modal, Figure 7(b). The kurtosis of d_3 complements m.a.(3,4) as a chatter indicator.

Gaussian wavelet transforms were employed in reference [5] in the study of non-regenerative thread and slot cutting processes. Identification of cutting states was based on qualitative features of wavelet based time-scale plots. Quantitative cutting state indicators were not given. The properties of m.a.(3,4) suggest that it may find application in the control of orthogonal cutting.

ACKNOWLEDGMENTS

The authors acknowledge the support of D.O.E. through DE-FG02-93-ER14335 and the N.S.F. through GER-9354956. The encouragement of D. Manley, of the D.O.E. and of P. Grootenhuis and D. J. Ewins, of Imperial College of Science and Technology, London, is appreciated.

REFERENCES

1. J. Tlusty 1979 *CIRP Annals* **27**, 583–589. Analysis of the state of research in cutting dynamics.
2. J. S. Lin and C. I. Weng 1990 *International Journal of Machine Tools and Manufacturing* **30**, 53–64. A nonlinear model of cutting.
3. D. W. Wu and C. R. Liu 1985. *Transactions of the American Society of Mechanical Engineers, Journal of Engineering for Industry* **107**, 107–118. An analytical model of cutting dynamics, parts 1 and 2.
4. I. N. Tansel, A. Wagiman and T. Tziranir 1991 *International Journal of Machine Tools and Manufacturing* **31**, 539–552. Recognition of chatter with neural networks.
5. M. K. Khraishen, C. Pezeshki and A. E. Bayoumi 1995 *Journal of Sound and Vibration* **180**, 67–87. Time series based analysis for primary chatter in metal cutting.
6. B. S. Berger, I. Minis *et al*. 1997 *Journal of Sound and Vibration* **200**, 15–29. Cutting state identification.
7. A. Cohen, I. Daubechies and J. C. Feauveau 1990 *Communications on Pure and Applied Mathematics* **45**, 485–560. Biorthogonal bases of compactly supported wavelets.
8. I. Daubechies 1992 *Ten Lectures on Wavelets*. Philadelphia, PA: Society for Industrial and Applied Mathematics.
9. M. Vetterli and C. Herley 1993 *IEEE Transactions on Signal Processing* **IT-41**, 2536–2556. Wavelets and recursive filter banks.
10. M. Misiti, Y. Misiti, G. Oppenheim and J. M. Poggi 1996 *Wavelet Toolbox*. Natick, MA The Math Works Inc.
11. G. Strang and T. Nguyen 1996 *Wavelets and Filter Banks* Wellesley MA: Wellesley–Cambridge Press.

APPENDIX: NOMENCLATURE

A_N	reconstructed approximation at level N
d_i	reconstructed detail at level i
f	frequency coefficient
$f(t), f(n)$	continuous signal, discrete signal
γ_2	kurtosis
m.a.(a, b)	mean absolute deviation of detail a divided by the mean absolute deviation of detail b
m_o	linear phase filter
md.a.(a, b)	median absolute deviation of detail a divided by the median absolute deviation of detail b
$\sigma(a, b)$	standard deviation of detail a divided by the standard deviation of detail b
t	time
ω	frequency (rad/s)
ψ, ϕ	wavelet function, scaling function
ψ_{jk}, ϕ_{jk}	wavelet and scaling functions at level k and scale j
bi 6,8	biorthogonal wavelets with spline 6,8
$\phi_i\ (t)$	uniformly distributed random variables